

# Time-dependent phase shift of a retrieved pulse in off-resonant electromagnetically-induced-transparency-based light storage

M.-A. Maynard, R. Bouchez, J. Lugani, F. Bretenaker, F. Goldfarb, and E. Brion

*Laboratoire Aimé Cotton, Université Paris-Sud, ENS Cachan, CNRS, Université Paris-Saclay, 91405 Orsay Cedex, France*

(Received 21 July 2015; published 2 November 2015)

We report measurements of the time-dependent phases of the leak and retrieved pulses obtained in electromagnetically-induced-transparency storage experiments with metastable helium vapor at room temperature. In particular, we investigate the influence of the optical detuning at two-photon resonance and provide numerical simulations of the full dynamical Maxwell-Bloch equations, which allow us to account for the experimental results.

DOI: [10.1103/PhysRevA.92.053803](https://doi.org/10.1103/PhysRevA.92.053803)

PACS number(s): 42.50.Gy, 42.50.Ex, 42.50.Md

## I. INTRODUCTION

Because they do not interact with each other and can be guided via optical fibers over long distances with relatively low losses, photons appear as ideal information carriers and are therefore put forward as the “flying qubits” in most quantum communication protocols. The design of memories able to reliably store and retrieve photonic states is, however, still an open problem. The most commonly studied protocol, considered to implement such a quantum memory, is electromagnetically induced transparency (EIT) [1]. This protocol was implemented in various systems such as cold atoms, gas cells, and doped crystals [2–4]. Although the Doppler broadening might seem to lead to strong limitations, EIT-based light storage in warm alkali vapors gives good results and is still a subject of active investigation [5]. In recent years, some experiments were also performed in a Raman configuration, using pulses which are highly detuned from the optical resonances in gas cells [6–8].

The EIT-based storage protocol in a  $\Lambda$  atomic system relies on the long-lived Raman coherence between the two ground states which are optically coupled to the excited level. When a strong-coupling beam is applied along one of the two transitions, a narrow transparency window limited by the Raman coherence decay rate is opened along the other leg of the system. Because of the slow-light effect associated with such a dramatic change of the medium absorption properties, a weak probe pulse on the second transition is compressed while propagating through the medium. When this pulse has fully entered the atomic medium, it can be mapped onto the Raman coherences which are excited by the two-photon process by suddenly switching off the coupling beam. It can be safely stored during times smaller than the lifetime of Raman coherence. Finally, the signal pulse can be simply retrieved by switching on the coupling beam again. In the Raman configuration, the coupling and probe pulses are optically far off-resonance but still fulfill the two-photon transition condition. The advantage is a large bandwidth that allows us to work with data rates higher than in the usual EIT regime [6].

Atoms at room temperature in a gas cell are particularly attractive for light storage because of the simplicity of their implementation. The effects of the significant Doppler broadening can be minimized using copropagating coupling and probe beams, so that the two-photon resonance condition can be verified for all velocity classes: all the atoms can

thus participate in the EIT phenomenon as soon as they are pumped in the probed level. As a consequence, handy simple gas cells have turned out to be attractive for slow-light or even stopped-light experiments [5]. In a previous work [9], we reported on an added phase shift recorded for EIT-based light-storage experiments carried out in a helium gas at room temperature when the coupling beam is detuned from the center of the Doppler line. The simple model that we have derived could not satisfactorily account for our observations that were recorded for intermediate detunings, e.g., close to the Doppler broadening of the transition. In the present paper, we come back to this problem and provide new experimental results, i.e., time-dependent measurements of the retrieved signal phase shift, as well as numerical results obtained through the simulation of the full system of Maxwell-Bloch equations. The behavior of these phase shifts with the coupling detuning seems to be satisfactorily accounted for by our simulations. We also perform numerical calculations in the Raman regime.

This paper is organized as follows. In Sec. II we present the system and setup and describe how to measure the time-dependent phase shift of the retrieved pulse with respect to the coupling beam. We also briefly review the system of Maxwell-Bloch equations which governs our system and describe their numerical integration. In Sec. III, we provide our experimental and numerical results and show that they qualitatively agree. We also apply our simulations to the far-off-resonant Raman case. Finally, we conclude in Sec. IV and give possible perspectives of our work.

## II. EXPERIMENTAL SETUP AND NUMERICAL SIMULATIONS

### A. EIT storage experimental setup

The atoms preferably used for EIT storage experiments are alkali atoms, mainly rubidium and sometimes sodium or cesium. We choose here to work with metastable  $^4\text{He}$  atoms, which have the advantage of a very simple structure without hyperfine levels: transitions are thus far enough from one another to investigate the effect of detunings of the coupling and probe beams on light storage and retrieval. We, however, think our results also apply, at least qualitatively, to the behavior of EIT experiments carried out with the species mentioned above in the far-detuned regime [6–8].

In our setup represented in Fig. 1, a 6-cm-long cell is filled with 1 Torr of helium atoms which are continuously excited

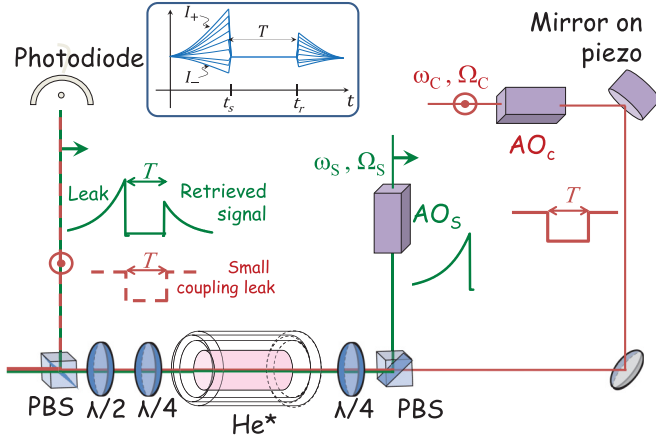


FIG. 1. (Color online) Experimental setup for EIT storage in metastable helium. The coupling and signal beams are derived from the same laser diode. They are initially linearly and orthogonally polarized, of optical frequencies  $\omega_c$  and  $\omega_s$  and Rabi frequencies  $\Omega_c$  and  $\Omega_s$ , respectively. Acousto-optic modulators are used to control the frequencies and amplitudes of the beams. Polarizing beam splitters (PBS) allow us to separate or recombine the beams. Circular orthogonal polarizations are obtained by a quarter-wave plate. The cell is contained in a  $\mu$ -metal shielding. After the cell, polarization optics select mainly the probe beam with some remaining coupling beam. The phase of the coupling beam is scanned thanks to a mirror on a piezoelectric transducer.

to their metastable state  $2^3S_1$  by a rf discharge at 27 MHz. Each of the metastable ground states  $|2^3S_1, m_J = 0, \pm 1\rangle$  is hence fed with the same rate, denoted by  $\frac{\Lambda}{3}$ . The cell is isolated from magnetic field gradients by a three-layer  $\mu$ -metal shield to avoid spurious dephasing effects on the different Zeeman components. A strong circularly polarized field, called the control beam, propagates along the quantization axis  $z$ . Its power is set at 18 mW for a beam diameter of 3 mm. As shown in Fig. 2, the coupling field drives the transitions  $|2^3S_1, m_J = -1\rangle \leftrightarrow |2^3P_1, m_J = 0\rangle$  and  $|2^3S_1, m_J = 0\rangle \leftrightarrow |2^3P_1, m_J = 1\rangle$ . Owing to the spontaneous transitions  $|2^3P_1, m_J = 0\rangle \rightarrow |2^3S_1, m_J = \pm 1\rangle$  and

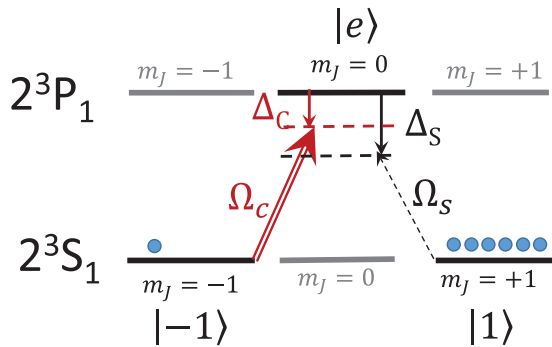


FIG. 2. (Color online) Atomic structure scheme for the D1 transition of metastable helium. The relevant states which constitute the three-level  $\Lambda$  system are shown in black.  $\Delta_c$  and  $\Delta_s$  are the optical detunings, and  $\Omega_c$  and  $\Omega_s$  are the Rabi frequencies of the coupling and signal beams, respectively. The two-photon resonance is achieved for  $\Delta_c = \Delta_s$ .

$|2^3P_1, m_J = 1\rangle \rightarrow |2^3S_1, m_J = 0, 1\rangle$ , the atoms end up in the state  $|1\rangle \equiv |2^3S_1, m_J = 1\rangle$  within a few pumping cycles after the coupling beam has been switched on. As the atoms are at room temperature, the Doppler broadening in the cell is  $\omega_D/2\pi \approx 1$  GHz. We denote by  $\Delta_c \equiv \omega_c - \omega_0$  the detuning of the coupling frequency  $\omega_c$  with respect to the natural frequency  $\omega_0/(2\pi) \approx 2.8 \times 10^{14}$  Hz of the transition  $2^3S_1 \leftrightarrow 2^3P_1$  at the center of the Doppler line.

Once optical pumping is achieved, a weak signal pulse is sent through the atomic medium along the  $z$  axis. Its polarization is circular and orthogonal to that of the coupling beam: the signal therefore couples state  $|1\rangle$  to  $|e\rangle \equiv |2^3P_1, m_J = 0\rangle$ , and we denote by  $\Delta_s \equiv \omega_s - \omega_0$  the detuning of the signal frequency  $\omega_s$  from the center of the Doppler profile. Both signal and coupling beams are derived from the same laser diode, and their frequencies and amplitudes are controlled by two acousto-optic modulators. Due to the efficiency of optical pumping through the coupling beam, we assume that the state  $|2^3S_1, m_J = 0\rangle$  remains essentially unpopulated during the whole process, and we accordingly neglect the driving of the transition  $|2^3S_1, m_J = 0\rangle \leftrightarrow |2^3P_1, m_J = -1\rangle$  by the signal field. Submitted to the coupling and signal fields, the atoms therefore essentially evolve in the three-level  $\Lambda$  system  $\{|-1\rangle \equiv |2^3P_1, m_J = -1\rangle, |e\rangle, |1\rangle\}$  (see Fig. 2) as long as the detunings  $\Delta_{c,s} = \omega_{c,s} - \omega_0$  of the coupling and signal fields, respectively, are small enough to avoid exciting neighboring transitions. Thanks to the absence of hyperfine structure, the range of allowed values for  $\Delta_{c,s}$  is, however, much larger than in alkali vapor experiments: indeed, on the positive detuning side the nearest state ( $^3P_0$ ) is 30 GHz away from optical resonance  $\Delta_{c,s} = 0$ , while on the negative detuning side, the nearest state ( $^3P_2$ ) is 2.29 GHz away.

Under EIT conditions, the coupling beam opens a transparency window for the weak signal beam, which can therefore propagate without absorption through the medium if its spectrum is not too wide [10]. In the experimental results we present hereafter, we used a signal pulse, which consists of a smoothly increasing exponential followed by an abruptly decaying exponential of respective characteristic times  $2\mu\text{s}$  and 150 ns. Its maximum power is about  $170\mu\text{W}$ , and the beam diameter is about 3 mm. Different dissipative mechanisms influence the width of the EIT window besides spontaneous emission, such as collisions and transit of the atoms in and out of the beams. These phenomena result in the decay of atomic coherences at the rates  $\gamma_{-11}/2\pi \approx 14$  kHz for the Raman coherence  $\sigma_{-11}$  and  $\gamma_{e1}/2\pi \approx 22.8$  MHz for the optical coherence  $\sigma_{e1}$ . We have shown previously that velocity-changing collisions redistribute the pumping of the atoms over an effective width slightly smaller than the Doppler linewidth [11]. Under our conditions, with a coupling power of 18 mW, this effective width is experimentally estimated to be  $\Gamma_D/2\pi \approx 0.8$  GHz. Due to power broadening, the width of the transparency window is then of the order of 500 kHz.

The highly dispersive character of the medium under EIT conditions can be used furthermore to store and retrieve a weak signal pulse: due to EIT dispersion, the signal pulse indeed travels with a reduced group velocity and is temporally contracted. Once the pulse has entered the cell, the coupling beam can be switched off: information about the signal pulse is then stored in the Raman coherences. After a storage time  $T$ ,

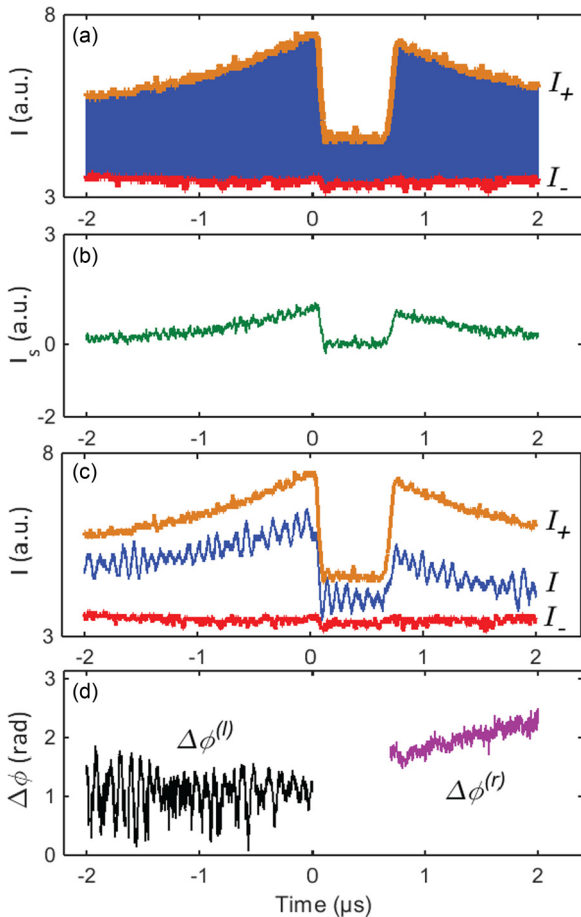


FIG. 3. (Color online) Experimental plots showing the data-processing steps. The coupling beam is switched off between times  $t = 0$  and  $t = 0.6 \mu\text{s}$ . The optical detunings are set at  $\Delta_{c,s} = 1 \text{ GHz}$ . The same vertical scale is used in (a), (b), and (c). (a) Accumulated plot of the interference signal  $I(t)$  between the probe and coupling beams. Upper and lower envelopes  $I_{\pm}(t)$  are shown in orange (light gray) and red (medium gray), respectively. (b) Signal intensity  $I_s(t)$  at the exit of the cell, deduced from the previous accumulated plot (a) and from a measurement of the coupling intensity  $I_c$ . (c) Interference signal  $I(t)$  between the probe and coupling beams [blue (dark gray) curve]. It is contained between the upper and lower envelopes  $I_{\pm}(t)$ , shown in orange (light gray) and red (medium gray), respectively. One can note the presence of spurious oscillations generated by the acousto-optic modulators. (d) Relative phases  $\Delta\phi^{(l)}(t)$  (black, left) and  $\Delta\phi^{(r)}(t)$  (purple, right) between the signal and coupling beams on the writing and retrieval parts, respectively. Notice that  $\Delta\phi^{(l)}(t)$  is indeed constant.

the control beam is switched on again, which releases the signal from the atomic coherence and ensures EIT absorption-free propagation. Note that in our experimental setup, the optical depth is only about 3.5, and the pulse can thus not be fully compressed in the cell. Due to the finite width of the transparency window and the finite length of the cell, a part, typically 10% of the incoming signal energy, leaks out before the coupling beam is turned off and the storage period begins [5]. A typical experimental record is given in Fig. 3(b). The first part of the detected signal is the leak, and after a storage time  $T \approx 0.6 \mu\text{s}$ , once the coupling beam is turned on again, the retrieved signal is clearly visible.

## B. Phase measurement setup

In [9], we investigated the relative phase  $\Delta\phi$  of the signal with respect to the coupling beam and showed the existence of an optical-detuning-dependent extra phase shift  $\varphi_{EIT}$  between the incident and retrieved pulses. This quantity can be measured through mixing the signal emerging from the cell with a small fraction of the control beam via polarization optics. The resulting intensity thus takes the form

$$I = I_c + I_s + \alpha\sqrt{I_c I_s(t)} \cos[\Delta\phi]. \quad (1)$$

In Eq. (1), the contrast factor  $\alpha$ , which ideally equals 2, accounts for nonperfect alignment of the beams and is measured for each set of data.  $I_c$  denotes the intensity of the small fraction of the coupling field which is mixed and interferes with the signal field. It takes the same constant value  $I_c$  during the writing and retrieval periods, while it vanishes during the storage time. The value  $I_c$  is measured in the absence of the signal (one assumes that the introduction of the signal pulse does not substantially affect the measurement of  $I_c$ ). The phase of the coupling beam is varied via a piezoelectric actuator from one experimental run to another: the scan is slow enough that it is assumed to be constant during both the writing and retrieval steps.  $I_s(t)$  is the time-dependent intensity of the signal beam emerging from the cell. We denote by  $I_s^{(l)}(t)$  and  $I_s^{(r)}(t)$  the intensities of the leak and retrieved pulses, respectively. Accordingly, we introduce  $\Delta\phi^{(l)}(t)$  and  $\Delta\phi^{(r)}(t)$ , the relative phases of the leak and retrieved pulses with respect to the coupling beam.

To obtain the extra phase shift  $\varphi_{EIT}$  between the incident and retrieved pulses, we measure the relative phases  $\Delta\phi^{(l)}$ ,  $\Delta\phi^{(r)}$  by homodyne detection. Repeating the same writing-storage-retrieval sequence for many different positions of the piezoelectric actuator, we obtain an accumulated plot whose upper and lower envelopes correspond, respectively, to  $I_{\pm}(t) = I_c + I_s(t) \pm \alpha\sqrt{I_c I_s(t)}$  [see Fig. 3(a)]. Given the previously measured value of  $I_c$ , one can infer  $I_s(t)$  from  $(I_+ + I_-)$  and  $\alpha$  from  $(I_+ - I_-)$  [see Fig. 3(b)]. For a given position of the piezoactuator, one can then obtain  $\Delta\phi^{(l)}(t)$  and  $\Delta\phi^{(r)}(t)$  through fitting the experimental record with Eq. (1) at each time  $t$  [see Figs. 3(c) and 3(d)]. It was verified both experimentally and numerically that the phase of the leak is constant [ $\Delta\phi^{(l)}(t) \equiv \Delta\phi^{(l)}$ ] and can therefore be taken as a reference for the time-dependent relative phase of the retrieved pulse  $\Delta\phi^{(r)}(t)$ . This time independence of the leak phase is ensured by the fact that its spectral content is much narrower than the EIT bandwidth. This is obtained thanks to the shape of the signal pulse: a slow exponential increase, followed by a sharp decrease. The part of the pulse which contains only low frequencies enters first and gives form to a leak, whose phase is constant. The “extra phase shift” is then measured as  $[\Delta\phi^{(r)}(t) - \Delta\phi^{(l)}] \equiv \varphi_{EIT}(t)$ . Let us stress that in [9], we assumed that the relative phases  $\Delta\phi^{(l,r)}$  of the leak and retrieved pulses were time independent: therefore, we directly extracted effective “averaged” values for  $\alpha$  and  $\varphi_{EIT}$  by performing a two-parameter fit of the data with Eq. (1). Here, by contrast, we measure the time dependence of the phases and provide experimental plots for  $\varphi_{EIT}(t)$  without any assumption of its behavior.

### C. Numerical simulation principles

For numerical simulations, we described the system in the one-dimensional approximation. On the dimensions of the atomic sample, the coupling and probe transverse profiles are assumed to remain constant. These fields can therefore be cast under the form

$$\mathbf{E}_{c,s}(z,t) = \text{Re}[\mathcal{E}_{c,s}(z,t)\mathbf{e}_{\pm}e^{-i(\omega_{c,s}t - k_{c,s}z)}],$$

where  $\mathcal{E}_{c,s}(z,t)$  denote the respective slowly varying amplitudes of the control and signal fields,  $\omega_{c,s}$  and  $k_{c,s}$  stand for their respective frequencies and wave numbers, and  $\mathbf{e}_{\pm} \equiv (\mathbf{e}_x \pm i\mathbf{e}_y)/\sqrt{2}$  ( $\mathbf{e}_x$  and  $\mathbf{e}_y$  define an arbitrary basis in the plane perpendicular to the propagation direction  $\mathbf{e}_z$ ).

Following, e.g., [12], we model the atomic sample as a continuous medium of uniform linear density  $n_{at}$  and define the average density matrix of the slice  $[z, z + \Delta z]$  by

$$\hat{\sigma}(z,t) \equiv \frac{1}{n_{at}\Delta z} \sum_{z \leq z_i \leq z + \Delta z} \hat{\sigma}_i(t).$$

We moreover define the density matrix elements  $\sigma_{ij} = \langle i|\hat{\sigma}|j\rangle$ , where  $i, j$  refer to the atomic levels and can take the values  $-1, 1$ , or  $e$  (see Fig. 2). We introduce the slowly varying coherences  $\tilde{\sigma}_{e1}$ ,  $\tilde{\sigma}_{e-1}$ , and  $\tilde{\sigma}_{-11}$ , defined by

$$\tilde{\sigma}_{e1} = e^{i\omega_s(t - \frac{z}{c})}\sigma_{e1},$$

$$\tilde{\sigma}_{e-1} = e^{i\omega_e(t - \frac{z}{c})}\sigma_{e-1},$$

$$\tilde{\sigma}_{-11} = e^{i\Delta_R(t - \frac{z}{c})}\sigma_{-11},$$

and write the Bloch equations in the rotating-wave approximation for the class of velocity which is at the center of the Doppler profile:

$$\partial_t \sigma_{-1-1} = \frac{\gamma_t}{3} - \gamma_t \sigma_{-1-1} + \frac{\Gamma_0}{2} \sigma_{ee} + i(\Omega_c^* \tilde{\sigma}_{e-1} - \Omega_c \tilde{\sigma}_{-1e}), \quad (2)$$

$$\partial_t \sigma_{ee} = -(\Gamma_0 + \gamma_t) \sigma_{ee} + i(\Omega_c \tilde{\sigma}_{-1e} - \Omega_c^* \tilde{\sigma}_{e-1} + \Omega_s \tilde{\sigma}_{1e} - \Omega_s^* \tilde{\sigma}_{e1}), \quad (3)$$

$$\partial_t \sigma_{11} = \frac{2\gamma_t}{3} - \gamma_t \sigma_{11} + \frac{\Gamma_0}{2} \sigma_{ee} + i(\Omega_s^* \tilde{\sigma}_{e1} - \Omega_s \tilde{\sigma}_{1e}), \quad (4)$$

$$\partial_t \tilde{\sigma}_{-11} = -(\gamma_{-11} - i\Delta_R) \tilde{\sigma}_{-11} + i(\Omega_c^* \tilde{\sigma}_{e1} - \Omega_s \tilde{\sigma}_{-1e}), \quad (5)$$

$$\partial_t \tilde{\sigma}_{-1e} = -(\gamma_{-1e} + i\Delta_c) \tilde{\sigma}_{-1e} + i[\Omega_c^* (\sigma_{ee} - \sigma_{-1-1}) - \Omega_s^* \tilde{\sigma}_{-11}], \quad (6)$$

$$\partial_t \tilde{\sigma}_{1e} = -(\gamma_{1e} + i\Delta_s) \tilde{\sigma}_{1e} + i\{\Omega_s^* (\sigma_{ee} - \sigma_{11}) - \Omega_c^* \tilde{\sigma}_{-11}\}. \quad (7)$$

Here,  $\Gamma_0$  is the population decay rate of state  $|e\rangle$ , and the Rabi frequencies  $\Omega_{c,s}$  are defined by

$$\hbar\Omega_{c,s} \equiv \frac{1}{2}d_{c,s}\mathcal{E}_{c,s}(z,t),$$

where  $d_{c,s} \equiv \langle e|\hat{\mathbf{d}} \cdot \mathbf{e}_{\pm}|\mp 1\rangle$  are the relevant matrix elements of the dipole operator  $\hat{\mathbf{d}}$ .

To take into account all the atoms that are distributed in different velocity classes over the Doppler linewidth, we developed a simple model in which the optical coherence

decay rates  $\gamma_{1e} = \gamma_{-1e}$  are replaced by the effective Doppler width  $\Gamma_D$ . This gives satisfactory results thanks to the redistribution of the pumping by velocity-changing collisions [13,14]. All our simulations were performed using this purely homogeneous broadening model. Consequently, we call  $\Delta_{c,s}$  the optical detuning, implicitly defined with respect to the center of the Doppler profile.

To ensure that the full population remains constant, the discharge-assisted ground-state feeding rate  $\Lambda$  has been set to  $\gamma_t$ , the transit rate of the atoms through the laser beam. Moreover, while state  $|-1\rangle$  is fed with the rate  $\frac{\Lambda}{3} = \frac{\gamma_t}{3}$ , state  $|1\rangle$  is effectively fed with the rate  $\approx \frac{2\Lambda}{3} = \frac{2\gamma_t}{3}$ . As can be checked by considering the full six-level system including not only the  $\Lambda$  system of interest but also states  $|2^3S_1, m_J = 0\rangle, |2^3P_1, m_J = \pm 1\rangle$ , state  $|1\rangle$  is indeed directly fed by the rf discharge with the rate  $\frac{\Lambda}{3}$  and also indirectly via state  $|2^3S_1, m_J = 0\rangle$ , whose population is (almost) immediately transferred to  $|1\rangle$  through optical pumping.

Finally, in the medium, the fields propagate according to the Helmholtz equation, written in the slowly varying envelope approximation

$$\left(\frac{\partial}{\partial z} + \frac{1}{c}\frac{\partial}{\partial t}\right)\Omega_{c,s}(z,t) = i\eta_{c,s}\tilde{\sigma}_{e\mp 1}(z,t), \quad (8)$$

where  $\eta_{c,s} \equiv (n_{at}k_{c,s}|d_{c,s}|^2)/(2\hbar\epsilon_0)$ .

The set of Maxwell-Bloch equations Eqs. (2)–(8) was numerically solved in MATLAB using the Lax discretization method [15]. The medium was split into 100 spatial steps of 0.6 mm, while the whole storage-retrieval sequence was split into  $6 \times 10^6$  time steps of 2 ps. We present and discuss our numerical results in the following section.

### III. RESULTS AND DISCUSSION

All the experimental results and simulations are performed at two-photon resonance, which means that the coupling and signal optical detunings are equal. Figure 4 shows

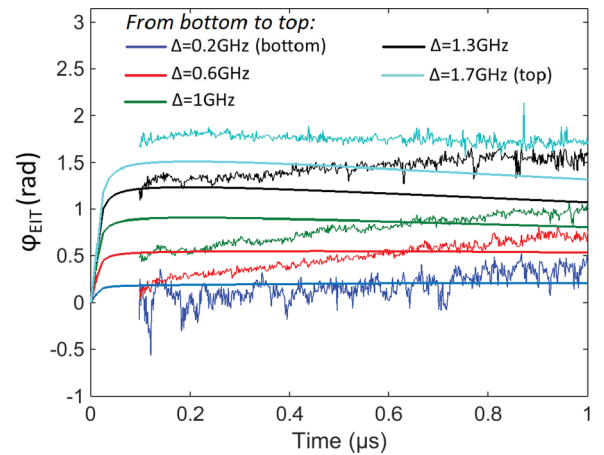


FIG. 4. (Color online) Temporal evolution of the extra phase shift  $\varphi_{EIT}(t)$ . Experimental data, recorded from bottom to top, for  $\Delta = 0.2$  GHz (blue, bottom), 0.6 GHz (red), 1 GHz (green), 1.3 GHz (black), and 1.7 GHz (cyan, top). Corresponding simulations are shown as solid lines. The time origin corresponds to the beginning of the retrieval, when the coupling is switched on again. The storage time is set at  $T = 0.6 \mu\text{s}$ .

experimental records for the time-dependent extra phase shift  $\varphi_{EIT}(t)$ , achieved with different values of the optical detunings  $\Delta = \Delta_c = \Delta_s$ , between 0 and 2 GHz. The detunings are set here on the positive side, where the nearest state ( $^3P_0$ ) is nearly 30 GHz away. Each curve is obtained after averaging over 15 sets of data, recorded at different times, for different positions of the homodyne-detection piezoactuator. The traces recorded on the oscilloscope present some spurious oscillations at a period of about 90 ns. This noise is generated by the acousto-optic modulators and could be removed by numerically filtering the spurious frequencies during the data processing. In Fig. 4, the time origin corresponds to the beginning of the retrieval, when the coupling beam is turned on again. At that time, the probe intensity starts increasing to form the retrieved pulse. We plot only the evolution of the extra phase shift  $\varphi_{EIT}(t)$  when the signal intensity is high enough, typically from roughly 100 ns to 1  $\mu$ s after the start of the retrieval. One can see that  $\varphi_{EIT}(t)$  is not constant over the retrieval, and its magnitude increases with the optical detuning  $\Delta$ .

The experimental plots are compared with numerical simulations of the full Maxwell-Bloch equations derived as explained in the previous section. We first observe that both the order of magnitude of  $\varphi_{EIT}$  and its variations with  $\Delta$  qualitatively agree. Discrepancies are, however, more visible in the time dependence of  $\varphi_{EIT}(t)$ , particularly for the three intermediate curves ( $\Delta = 0.6, 1, 1.3$  GHz); however, as emphasized above, the order of magnitude of the phase shift is good, and its slope disagrees with theoretical predictions. One possible source for the observed discrepancies is our oversimplified treatment of the velocity distribution in the Doppler profile. Here, we indeed assumed that velocity-changing collisions are efficient enough to instantaneously and perfectly redistribute atoms pumped in the probed level  $|1\rangle$  over the effective Doppler profile so that all these atoms contribute coherently to the storage process as if the broadening were homogeneous. Although this approximation is commonly used (see [13,14]), it might be severely questioned here, especially in optically detuned conditions that change the thermal equilibrium. In particular, the absorption of the coupling beam measured experimentally could not be well reproduced by the simulations. This should also have an effect on the storage efficiency and on the temporal shape of the phase. Note that in the simulation program, in order to “minimize” this problem, we use an averaged coupling intensity over the length of the cell as the input parameter, instead of the real coupling intensity measured at the entrance of the cell. Note also that we have checked that our numerical results agree with the analytic approximate solutions presented in [12,16].

To understand better the physical origin of the extra phase shift  $\varphi_{EIT}(t)$ , we compared the time-dependent relative phase  $\Delta\phi(t)$  between the signal and coupling beams at the exit of the cell, obtained (i) during the storage and retrieval of a weak signal pulse [ $\Delta\phi(t) = \Delta\phi^{(l)}(t)$  before  $t = 0$  and  $\Delta\phi(t) = \Delta\phi^{(r)}(t)$  after the storage time  $T = 0.6 \mu$ s] and (ii) during the direct EIT propagation of the same weak pulse in the medium, while the coupling amplitude remained constant. To compute  $\Delta\phi(t)$  in case (i), we used the full simulation of the Maxwell-Bloch set of equations, whereas in case (ii) we simply propagated each spectral component  $\omega$  of the incoming pulse with the corresponding susceptibility  $\chi(\omega)$ .

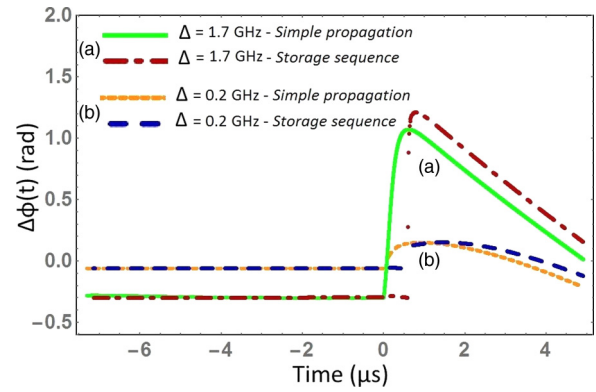


FIG. 5. (Color online) Temporal evolution of the relative phase  $\Delta\phi(t)$  during the direct propagation of a weak signal pulse through the medium under EIT conditions (“simple propagation”) and during the storage and retrieval of the same pulse (“storage sequence”) for two different optical detunings: (a) 1.7 GHz (green solid line and red dash-dotted line) and (b) 0.2 GHz (orange dotted line and blue dashed line). The time origin is arbitrarily chosen as the starting of the storage period.

Figure 5 simultaneously displays the results we obtained in both cases for two different values of the optical detuning,  $\Delta = 0.2, 1.7$  GHz. The shape and order of magnitude for  $\Delta\phi(t)$  are clearly the same in cases (i) and (ii): the main effect of the storage is to introduce a delay corresponding to the storage time  $T$ . Here, we chose  $T = 0.6 \mu$ s, but we checked both experimentally and theoretically that this phase shift does not depend on this storage time. This suggests that the observed extra phase shift  $\varphi_{EIT}$  originates almost exclusively from the asymmetric dispersion experienced by the pulse when propagating in the atomic medium under detuned EIT conditions. Indeed, the stored part presents a sharp decrease associated with many frequency components and is

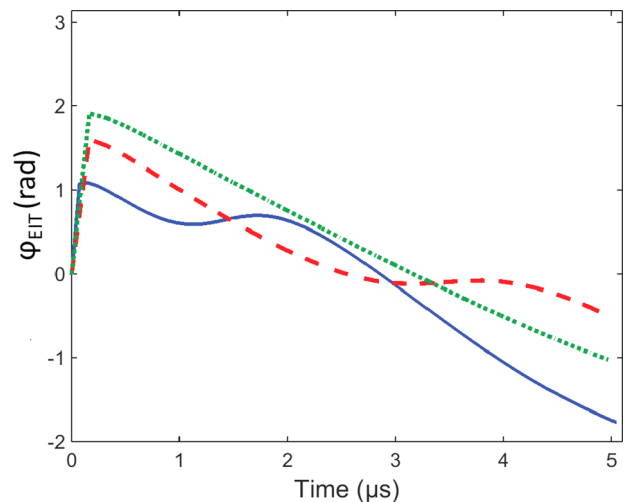


FIG. 6. (Color online) Temporal evolution of the phase shift  $\varphi_{EIT}(t)$  for different optical detunings in the Raman regime:  $\Delta = 10$  GHz (blue solid line),  $\Delta = 15$  GHz (red dashed line),  $\Delta = 20$  GHz (green dotted line). These curves are obtained with the full simulation of the Maxwell-Bloch set of equations, for ten times more atoms than in our experimental case, and for a coupling power of 200 mW. The time origin is chosen as the starting of the retrieval period.

thus very sensitive to dispersive effects. This problem should be taken into account for high-speed information applications, like experiments performed in the Raman configuration [6–8]. We have thus performed simulations in the far-detuned regime as presented in Fig. 6. The simulation results shown here are plotted for three different optical detunings,  $\Delta = 10$  GHz,  $\Delta = 15$  GHz,  $\Delta = 20$  GHz, much higher than the  $\Gamma_D \approx 0.8$  GHz Doppler broadening. They were obtained for a number of atoms  $n_{at}$  which is ten times higher than in our experimental case and for a coupling power of 200 mW. These simulation results demonstrate a similar effect on the retrieved signal pulse phase, even slightly stronger than in our experimental conditions. We checked that our numerical results in the Raman configuration agree with the analytic integral formula derived in the adiabatic approximation by Gorshkov *et al.* [12], which relates the outgoing field to the incoming one. Note that, although analytic, this formula does not lend itself to simple physical interpretations as far as the phase is concerned.

#### IV. CONCLUSION

In this paper, we have experimentally investigated a time-dependent extra phase shift that appears in a storage-retrieval experiment, performed in a room-temperature atomic cell in

optically detuned conditions. This phase shift varies with time and does not depend on the storage time. We have provided numerical simulations which qualitatively agree with the experimental results: in particular, it appears that the magnitude of the relative phase depends on the optical detuning, while its temporal shape is mainly given by the spectrum of the incoming pulse. We explain the existence of this extra phase by propagation effects that can be understood by a simple propagation model under EIT conditions with optically detuned beams. Discrepancies may be due to an approximate treatment of Doppler broadening in the cell.

The results presented here might be important, particularly for light-storage experiments performed in the far-detuned Raman regime, as reported in [7]. How these results translate into the regime of quantum light is an intriguing feature that we intend to address in a future work.

#### ACKNOWLEDGMENTS

The work of M.-A.M. is supported by the Délégation Generale l'Armement (DGA), France, and the work of J.L. is supported by Indo-French CEFIPRA funding. We also thank the labex PALM and the Région Ile de France DIM NANOK for funding.

- 
- [1] K.-J. Boller, A. Imamoglu, and S. E. Harris, *Phys. Rev. Lett.* **66**, 2593 (1991).
  - [2] C. Liu, Z. Dutton, C. H. Behroozi, and L. V. Hau, *Nature (London)* **409**, 490 (2001).
  - [3] D. F. Phillips, A. Fleischhauer, A. Mair, R. L. Walsworth, and M. D. Lukin, *Phys. Rev. Lett.* **86**, 783 (2001).
  - [4] M. P. Hedges, J. J. Longdell, Y. Li, and M. J. Sellars, *Nature (London)* **465**, 1052 (2010).
  - [5] I. Novikova, R. L. Walsworth, and Y. Xiao, *Laser Photonics Rev.* **6**, 633 (2012).
  - [6] K. F. Reim, J. Nunn, V. O. Lorenz, B. J. Sussman, K. C. Lee, N. K. Langford, D. Jaksch, and I. A. Walmsley, *Nature Photonics* **4**, 218 (2010).
  - [7] K. F. Reim, P. Michelberger, K. C. Lee, J. Nunn, N. K. Langford, and I. A. Walmsley, *Phys. Rev. Lett.* **107**, 053603 (2011).
  - [8] K. F. Reim, J. Nunn, X.-M. Jin, P. S. Michelberger, T. F. M. Champion, D. G. England, K. C. Lee, W. S. Kolthammer, N. K. Langford, and I. A. Walmsley, *Phys. Rev. Lett.* **108**, 263602 (2012).
  - [9] M.-A. Maynard, T. Labidi, M. Mukhtar, S. Kumar, R. Ghosh, F. Bretenaker, and F. Goldfarb, *Europhys. Lett.* **105**, 44002 (2014).
  - [10] M. Fleischhauer, A. Imamoglu, and J. P. Marangos, *Rev. Mod. Phys.* **77**, 633 (2005).
  - [11] J. Ghosh, R. Ghosh, F. Goldfarb, J.-L. Le Gouët and F. Bretenaker, *Phys. Rev. A* **80**, 023817 (2009).
  - [12] A. V. Gorshkov, A. André, M. D. Lukin, and A. S. Sørensen, *Phys. Rev. A* **76**, 033805 (2007).
  - [13] F. Goldfarb, J. Ghosh, M. David, J. Ruggiero, T. Chaneïère, J.-L. Le Gouët, H. Gilles, R. Ghosh, and F. Bretenaker, *Europhys. Lett.* **82**, 54002 (2008).
  - [14] E. Figueroa, F. Vewinger, J. Appel, and A. I. Lvovsky, *Opt. Lett.* **31**, 2625 (2006).
  - [15] W. H. Press, S. A. Teukolsky, T. Vetterling, and B. P. Flannery, *Numerical Recipes in C* (Cambridge University Press, Cambridge, 1988).
  - [16] A. V. Gorshkov, A. André, M. Fleischhauer, A. S. Sørensen, and M. D. Lukin, *Phys. Rev. Lett.* **98**, 123601 (2007).